

Cite this: *Phys. Chem. Chem. Phys.*, 2012, **14**, 2501–2507

www.rsc.org/pccp

PAPER

# Internal energy deposition and ion fragmentation in atmospheric-pressure mid-infrared laser ablation electrospray ionization†

Peter Nemes,‡ Hehua Huang and Akos Vertes\*

Received 29th October 2011, Accepted 22nd December 2011

DOI: 10.1039/c2cp23411d

Mid-infrared laser ablation of water-rich targets at the maximum of the 2.94  $\mu\text{m}$  absorption band is a two-step process initiated by phase explosion followed by recoil pressure induced material ejection. Particulates and/or droplets ejected by this high temperature high pressure process can be ionized for mass spectrometry by charged droplets from an electrospray. In order to gauge the internal energy introduced in this laser ablation electrospray ionization (LAESI<sup>®</sup>) process, we apply the survival yield method and compare the results with electrospray ionization (ESI) and matrix-assisted laser desorption ionization (MALDI). The results indicate that LAESI yields ions with internal energies indistinguishable from those produced by ESI. This finding is consistent with the recoil pressure induced ejection of low micrometre droplets that does not significantly change the internal energy of solute molecules.

## 1. Introduction

Laser ablation (LA) at atmospheric pressure has gained considerable interest in biological investigations that span from basic research, material processing to medical intervention.<sup>1</sup> In the biophysical and bioanalytical sciences, controlled LA has found a successful application through laser capture microdissection that can selectively transfer minute amounts of biomaterials to short distances with a lateral resolution down to the subcellular level.<sup>2</sup> As most biological specimens contain an appreciable amount of water, special attention has been focused on mid-infrared (mid-IR) ablation at the strong 2.94  $\mu\text{m}$  absorption band of water that opens a way to manipulate and probe samples in the ambient environment. This absorption band is associated with the OH vibrations and is known to exhibit a nonlinearity at elevated energy densities.<sup>3</sup>

The ions, neutrals and particulates generated in atmospheric pressure laser desorption and ablation experiments are often utilized in ambient mass spectrometry<sup>4</sup> (MS) techniques. Among these rapidly evolving techniques, ultraviolet (UV) electrospray-assisted laser desorption ionization (ELDI),<sup>5</sup> atmospheric pressure matrix-assisted laser desorption ionization (MALDI)<sup>6–8</sup> and more recently laser ablation electrospray ionization

(LAESI<sup>®</sup>)<sup>9</sup> and its conceptual analogues, IR laser-assisted desorption electrospray ionization<sup>10</sup> and IR matrix-assisted laser desorption electrospray ionization,<sup>11</sup> have demonstrated direct ion production from biological targets. LAESI MS has proven particularly attractive for these samples because it relies on their native water as the energy coupling medium to perform mid-IR ablation. In addition, light penetration depth is typically higher in the mid-IR than in the UV region of the spectrum that in turn results in the ejection of more material. Applications range from lateral and three-dimensional chemical imaging of tissues<sup>12,13</sup> to the direct analysis of single cells.<sup>14–16</sup> Understanding these LA-based techniques, however, is dependent on exploring the fundamental processes in mid-IR LA of water-containing targets.

Mid-IR ablation of water-rich targets exhibits a complex spatiotemporal evolution that is fundamentally different in vacuum and at atmospheric pressure. In vacuum, expansion of the evaporation plume proceeds indefinitely, whereas atmospheric pressure conditions result in a finite stopping distance for the plume<sup>17</sup> and leads to two partially overlapping phases. Fast imaging experiments<sup>18</sup> and computational simulations<sup>19,20</sup> indicate that atmospheric pressure ablation, using laser pulses of nanosecond duration and 2.94  $\mu\text{m}$  wavelength, is initiated by rapid surface evaporation and phase explosion. As local temperatures in the sample reach 0.8 to 0.9 times the critical temperature (647 K in water), *i.e.*, 518 K to 582 K, within the first  $\sim 1 \mu\text{s}$  after irradiation,<sup>20</sup> these processes generate a dense plume consisting of a mixture of vapour and microscopic droplets that drives a shock-wave front at its interface with the ambient air (see Fig. 1(b) in ref. 18). A very small fraction of this plume consists of ions (the ion yield is below  $10^{-4}$ ), some of which can be directly detected.<sup>21</sup> Owing to the pressure

Department of Chemistry, The George Washington University, Washington, DC 20052, USA. E-mail: vertes@gwu.edu; Fax: +1-202-994-5873; Tel: +1-202-994-2717

† Electronic supplementary information (ESI) available: Additional survival yield curves, internal energy distributions, the critical bond energies, as well as the parameters obtained in the performed nonlinear regressions. See DOI: 10.1039/c2cp23411d

‡ Current address: US Food and Drug Administration, 10903 New Hampshire Ave. #64-3068, Silver Spring, MD 20993, USA. E-mail: Peter.Nemes@fda.hhs.gov; Tel: +1-301-796-3366

of the surrounding air, plume expansion is slowed down, and it comes to a halt at  $\sim 2$  mm above the sample surface.<sup>21</sup> Calculations suggest that as the plume collapses back onto the target, a fluence-dependent pressure of 500 to 900 MPa builds up within the surface layer that ultimately relaxes through the ejection of nanometre- to micrometre-sized particles. Particulates or droplets of the expelled material are only slowed by the drag force in the air, and thus projected up to 30 mm above the surface.<sup>18,21,22</sup> These theoretical and experimental studies also find that at atmospheric pressure molecules and ions do not travel to beyond 2–4 mm at even in the presence of electric fields. Based on this scenario it is unclear how much internal energy is deposited into the solutes in the droplets ejected from the sample.

In LAESI, the neutral projectiles generated in the second phase of the ablation are captured by the charged droplets of the electrospray and converted into gas-phase ions. Comparison of the corresponding mass spectra indicates that electrospray ionization (ESI) and LAESI yield ions with similar chemical composition and charge state, albeit with potential differences in ion yields.<sup>9</sup> This serves as partial evidence that, at least, the final steps of ion generation in LAESI are dictated by processes prevailing in ESI. Although vacuum-based mid-IR ablation has been long demonstrated to preserve macromolecular integrity in frozen samples<sup>23,24</sup> and ESI is widely known to result in low energy deposition into the generated ions,<sup>25,26</sup> high temperature and pressure conditions during atmospheric-pressure ablation may increase the internal energy of the solute molecules and cause their fragmentation. For example, lipid species have been reported to undergo dehydration in mid-IR ablation.<sup>27</sup> To what extent the high temperature and pressure conditions affect energy deposition into solutes during the ambient ablation process is unknown.

In this work, we gauged the internal energies of LAESI-generated ions using the survival yield method<sup>28,29</sup> for aqueous solutions and tissue samples and compared them to ions produced by ESI. The study involved a series of benzyl-substituted benzylpyridinium ions with a single decomposition channel and, therefore, provided a simplified method to correlate the amount of internal energy change with the degree of molecular fragmentation.<sup>25,30</sup> Our experiments were extended to biomolecules such as small peptides and vitamins. The obtained internal energies of ions produced by LAESI enabled comparisons with other ionization techniques, including MALDI,<sup>31–35</sup> laser-induced silicon microcolumn arrays (LISMA),<sup>36</sup> nanowires<sup>37</sup> and nanopost arrays (NAPA)<sup>38</sup> in vacuum, as well as ESI, paper spray,<sup>39</sup> desorption electrospray ionization (DESI),<sup>40</sup> and direct analysis in real time (DART)<sup>41</sup> at atmospheric pressure.

## 2. Experimental methods

### ESI source

Solutions of benzylpyridinium salts were prepared at 100 nM concentration with 50% methanol containing 0.1% acetic acid, and were supplied through a tapered tip metal emitter (100  $\mu\text{m}$  ID, New Objective, Woburn, MA) at 300 nL  $\text{min}^{-1}$  flow rate using a low-noise syringe pump (Physio 22, Harvard Apparatus, Holliston, MA). The emitter was positioned 10 mm from the sampling cone of the mass spectrometer,

and stable 3000 V generated by a high-voltage power supply (PS350, Stanford Research Systems, Inc., Sunnyvale, CA) was directly applied to it to achieve electrostatic spraying. The spray current was continuously monitored on the sampling cone of the mass spectrometer to indicate the absence of corona discharge. The average DC component of the current measured 22 nA.

### LAESI source

The LAESI source was similar to what had been reported elsewhere<sup>9</sup> and featured the same electrospray source as the one used in the ESI experiments described above. Briefly, a Nd:YAG laser-driven optical parametric oscillator (OPO) (Vibrant IR, Oportek Inc., Carlsbad, CA) provided laser pulses of 2.94  $\mu\text{m}$  wavelength and  $2.0 \pm 0.2$  mJ energy at repetition rates up to 10 Hz. This mid-IR beam was steered by gold mirrors and focused by a plano-convex ZnSe lens (Infrared Optical Products, Farmingdale, NY) on the sample surface 12 mm below the electrospray axis. At  $\sim 15$   $\text{J cm}^{-2}$  fluence, typical ablation craters in Japanese Spindle (*Euonymus japonicus*) leaves were circular and measured  $\sim 130$   $\mu\text{m}$  in diameter (see Fig. 1).

Solutions of the thermometer ions were deposited on glass microscope slides or air-dried onto the *E. japonicus* leaves at  $\sim 100$   $\mu\text{g cm}^{-2}$  density, and were immediately analysed. Importantly, in all LAESI experiments, alternative ion generation *via* atmospheric-pressure MALDI, ELDI, DESI, or direct ESI of particulate matter deposited on the electrospray emitter was carefully excluded.

When needed, sample cooling was achieved by a Peltier cooling stage operating at temperatures between 0  $^{\circ}\text{C}$  and  $-5$   $^{\circ}\text{C}$ . This unit was based on a ceramic thermoelectric module (Ferrotec Corp., Bedford, NH) coupled to a metal heat sink (Aavid Thermalloy, Concord, NH) using heat sink compound (GC Electronics, Rockford, IL) and glue (Henkel Loctite, Cleveland, OH), as well as two DC fans (Comair Rotron Co., San Diego, CA) to facilitate heat removal.

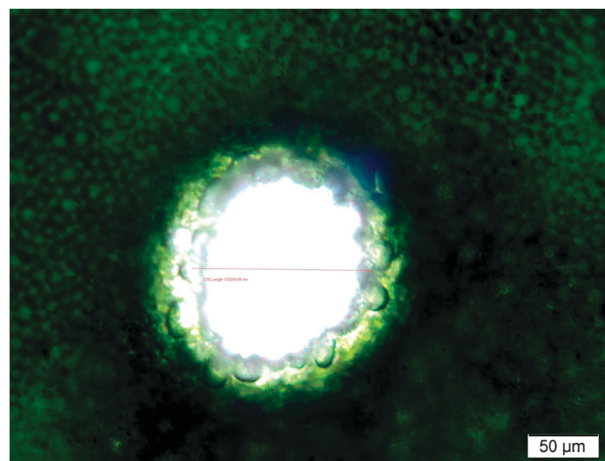


**Fig. 1** Optical microscope image of the laser–target interaction area on an *E. japonicus* leaf used for internal energy measurements indicates a 130  $\mu\text{m}$  diameter ablation spot after exposure to multiple mid-IR laser pulses of  $\sim 15$   $\text{J cm}^{-2}$  fluence.

## LAESI and ESI mass spectrometry

The produced charged droplets and ions were directly transferred through the atmospheric-pressure interface of a time-of-flight (TOF) mass spectrometer (AccuTOF JMST100LC, JEOL Ltd., Peabody, MA) and mass-analysed. Importantly, this instrument did not incorporate a collision-gas cell, so it allowed for direct ion transfer to the analyser without significantly affecting the internal energy of the ions.<sup>42,43</sup> The sampling cone of the mass spectrometer was maintained at 80 °C. All experimental variables were kept constant in the LAESI and ESI experiments to allow for direct comparison of the measured internal energies of the thermometer ions.

The influence of laser ablation rate and sample temperature on internal energy deposition was studied using a quadrupole TOF (Q-TOF) tandem mass spectrometer (Q-TOF Premier; Waters Co., Milford, MA). This instrument was also equipped with an atmospheric-pressure interface allowing the rapid sampling of LAESI- and ESI-generated charged species. For this system, a Nd:YAG laser-driven OPO (Opolette 100, Oportek, Carlsbad, CA) produced light pulses of 2.94  $\mu\text{m}$  wavelength at repetition rates of 10 Hz, 20 Hz, and 50 Hz. The cone voltage of this mass spectrometer was set to 8 V, while the collision energy was kept at 4 eV, necessary to ensure ion transfer through the collision cell to the detector with minimal collisional activation. In all MS experiments, data were collected for 2 min at a spectral acquisition rate of 1 Hz. Sample concentrations and the ion source settings were optimized to obtain ion signal intensity values between  $5 \times 10^4$  and  $5 \times 10^5$  counts per second, which ensured a linear detector response.

## MALDI mass spectrometry

MALDI studies were performed using a curved-field reflectron TOF mass spectrometer (Axima CFR, Shimadzu-Kratos, Manchester, UK) equipped with a nitrogen laser that emitted pulses at 337 nm wavelength and 4 ns pulse length (FWHM). The generated ions were analysed after delayed ion extraction, and mass spectra were averaged for 100 laser shots at a laser intensity of 85 arbitrary units.

## Chemicals and plant tissues

Benzyl-substituted benzylpyridinium salts, 4-nitro- (4NO<sub>2</sub>), 4-methyl- (4M), 4-chloro- (4Cl), 4-fluoro- (4F), 4-methoxy- (4MO), 3-methoxy- (3MO), 3-methyl- (3M) and 2-methyl- (2M), were custom synthesized by Celestial Specialty Chemicals (Nepean, Ontario, Canada). All other chemicals were purchased at gradient grade (solvents), reagent grade or higher (solutes) from Sigma-Aldrich Co. (St. Louis, MO) and were used without further purification. All samples in the ablation experiments were dissolved in the solvent and also used for the electrospray studies. For LAESI, peptide and vitamin B<sub>12</sub> solutions were prepared at 1  $\mu\text{M}$  and 800  $\mu\text{M}$  concentration, respectively. In the ESI experiments, these compounds were electrosprayed at 100 nM and 80  $\mu\text{M}$  concentrations, respectively. In the MALDI experiments, 800  $\mu\text{M}$  vitamin B<sub>12</sub> solution was mixed with 13 mM 2,5-dihydroxybenzoic acid (DHB) solution in equal volumes and was air-dried on stainless steel substrates at room temperature.

Fresh *E. japonicus* leaves were obtained from Washington, DC, between December 2010 and January 2011, and were directly used in the experiments.

## Hazards

General safety protocols were followed when handling flammable solvents and corrosive acid solutions. Protective laser safety goggles were worn at all times during the mid-IR LA experiments. High voltage connections were inspected for proper insulation, and exposed metal surfaces were grounded.

## 3. Results and discussion

Previous studies have established that the ion source and ion transfer conditions in mass spectrometers can alter the internal energy content of ions to varying degrees. For example, supersonic expansion results in analyte cooling as ions pass through the sampling cone in the first stage of a mass spectrometer.<sup>44</sup> In contrast, a gain of internal energy can be associated with acceleration (*e.g.*, by ion lenses) if the mean free path is shorter than the dimensions of these components. The propensity of ionized molecules to undergo fragmentation is further affected by the presence, type, and pressure of a collision gas, the temperature of incorporated components,<sup>26,45–48</sup> as well as the spraying mode of the electrospray source.<sup>49</sup> For this reason, the mass spectrometer interface parameters were optimized and kept constant throughout the experiments.

### Ion internal energies in LAESI of solutions

The ion transfer conditions of the mass spectrometers were characterized following the survival yield method.<sup>26,50</sup> Solutions of five thermometer ion salts (see Table S1, ESI<sup>†</sup>) were electrosprayed at increasing sampling cone-to-skimmer potentials, and the generated ions were mass-analysed. Ions with internal energies below the critical energy were detected as intact ions, whereas those with internal energies above the critical energy underwent unimolecular dissociation, resulting in the presence of both molecular and fragment ions with measurable ion signal intensities, IM and IF, respectively. The extent of molecular fragmentation was quantified by the survival yield, SY, that was defined as  $\text{SY} = \text{IM}/(\text{IM} + \text{IF})$  in accordance with the survival yield method.

Sigmoidal survival yield curves were measured for eight different thermometer ions as a function of their critical energies for five potential differences between the sampling and skimmer cones (the results are available in Fig. S1a, ESI<sup>†</sup>). Increasing potential differences shifted the internal energy distributions to higher means with increasing distribution widths (see Fig. S1b, ESI<sup>†</sup>), in agreement with earlier findings.<sup>25,51</sup> Potential differences of 50 and 60 V were selected for the comparison of ESI and LAESI because these values ensured a linear response between solute concentrations and ion signal intensities, relatively mild ion transfer conditions within the mass spectrometer, as well as acceptable nonlinear regression performance (regression coefficients > 0.9). As shown in Fig. 2(a), between 40 V and 60 V the survival yield data exhibited a relatively uniform distribution between the limiting 0 and 1 values corresponding to no and complete fragmentation, respectively. These measurements were repeated for the ESI ion

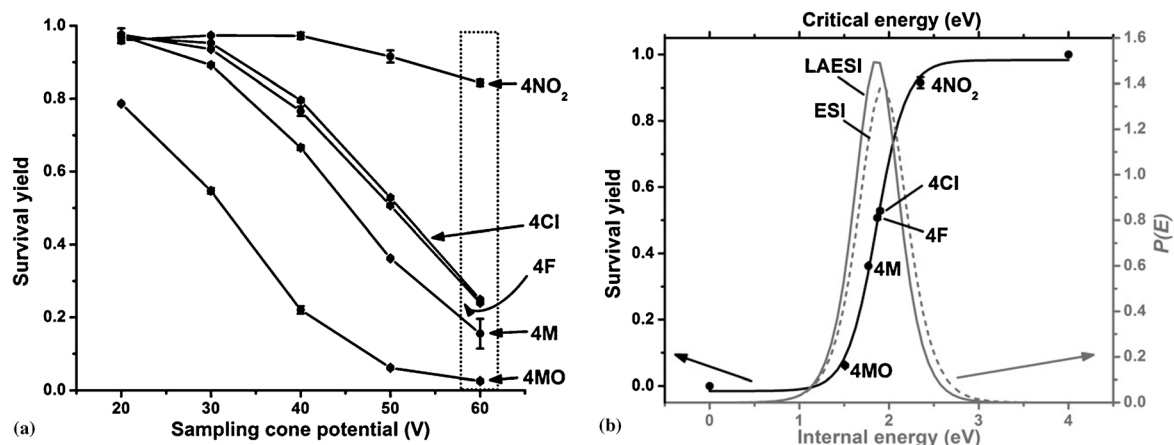


**Fig. 2** Internal energy deposition in mid-IR LAESI. (a) Survival yield experiments revealed optimal ion transfer conditions between 40 and 60 V sampling cone potentials, allowing the (b) deduction of the internal energy distribution,  $P(E)$ . At 50 V potential, ions generated in LAESI (axes and curve are in grey) and ESI (dotted grey curve) had similar internal energy distributions, both in shape and mean values. Nonlinear regression results are summarized in Table S2 (ESI<sup>†</sup>). Error bars are within symbols. These uncorrected internal energy values do not reflect the 'kinetic shift' but indicate relative changes.

source by spraying solutions of the thermometer ions. The acquired data revealed very similar results (data not shown) to LAESI and indicated that the overall energy deposition by LAESI resembled that of ESI. The compositional similarity of LAESI- and ESI-produced ions<sup>9</sup> further suggested that ion generation from charged droplets seeded with thermometer ions in LAESI occurred *via* processes similar to ESI.

The ion internal energy distributions were determined on the basis of the obtained survival yield data. As shown in Fig. 2(b) for LAESI, the measured survival yields, at, *e.g.*, 50 V cone voltage, rose with increasing critical energies<sup>26</sup> following the sigmoidal curve. Nonlinear regression was carried out using a Boltzmann function to represent the sigmoidal curve that resulted in an excellent fit with a correlation coefficient,  $r > 0.998$ . The first derivative of this curve, also shown in Fig. 2(b), provided the ion internal energy distribution,  $P(E)$ . For comparison the  $P(E)$  for ESI determined under identical conditions is also plotted in this figure. Noticeably, ions produced by LAESI and ESI exhibited very similar internal energy distributions. At a sampling cone potential of 50 V, the calculated averages of the distributions,  $\langle E \rangle$ , were 2.09 eV for ESI and 2.08 eV for LAESI (see Fig. 2(b)) with Gaussian widths of 0.52 and 0.49 eV, respectively.

Here, it is important to note that our measurements and calculations did not correct for the kinetic shift of the mass spectrometers, so the obtained energies were not absolute measures of the internal energy. For a given instrument and ion, however, the results could be used to directly compare the energy deposition processes between LAESI and ESI. Indeed, the ions produced from neutral particulates, ejected to distances over 10 mm, by LAESI were found to exhibit internal energies that were indistinguishable from the ones directly generated by ESI.

These results also provided mechanistic insight into the origin of LAESI-generated ions. The observed similarity in  $\langle E \rangle$  between LAESI and ESI suggested that the detected ions did not gain appreciable internal energy in the ablation process. This outcome, however, does not rule out that the chemical species

and particulates or droplets produced in the first phase ( $\sim 1 \mu\text{s}$ ) of the ablation exhibit higher internal energies due to the high temperature and pressure conditions during that period. Indeed, molecular decomposition had been observed to a limited extent in atmospheric pressure IR-MALDI experiments that collected ions closer to the surface ( $\sim 2 \text{ mm}$ ) produced directly by the ablation.<sup>21,52</sup> Those ions, however, are not detectable in LAESI experiments carried out at 12 mm from the surface (see Fig. 2(a) in ref. 21).

Our findings are consistent with a mechanism based on capturing the neutral projectiles, produced in the second phase of the ablation by recoil pressure induced ejection, by highly charged electrospray droplets. In order to assess the feasibility of this mechanism, let us estimate the stopping distance of the ejected droplets. Perpendicular to the ablated surface, the equation of motion for a droplet of initial velocity,  $v_0$ , of radius  $R$  and mass  $m$  decelerated by only the drag force,  $F(v)$ , assuming it follows Stokes law,  $F(v) = -cv$ , is:

$$x(t) = \frac{m}{c} v_0 \left[ 1 - \exp\left(-\frac{c}{m} t\right) \right] \quad (1)$$

where for a sphere  $c = 6\pi\mu R$  and  $\mu = 1.8 \times 10^{-5} \text{ kg m}^{-1} \text{ s}^{-1}$  is the dynamic viscosity of air at 25 °C. For water ablation by a Q-switched laser at  $5.4 \text{ J cm}^{-2}$  the initial velocity of the ejected droplets was found to be  $v_0 = 150 \text{ m s}^{-1}$ .<sup>18</sup> The Reynolds number for a  $2R = 10 \mu\text{m}$  diameter droplet departing at that velocity in ambient air of density  $\rho_{\text{air}} = 1.2 \text{ kg m}^{-3}$  is  $Re = 2R\rho_{\text{air}}v_0/\mu \approx 95$ , which is sufficiently low, so Stokes law can be used. Substituting the mass of spherical droplets and the expression for  $c$  into eqn (1) and taking its limit for very long times, the stopping distance of these droplets is

$$x_{\text{stop}}(t \rightarrow \infty) = 2\rho R^2 v_0 / 9\mu \quad (2)$$

where  $\rho$  is the density of the liquid, *i.e.*,  $\rho = 997 \text{ kg m}^{-3}$  for dilute aqueous solutions. For  $10 \mu\text{m}$  diameter water droplets departing at  $150 \text{ m s}^{-1}$ , the stopping distance comes to  $\sim 45 \text{ mm}$ . Considering the approximations we took in this estimate, the value is consistent with our finding that the

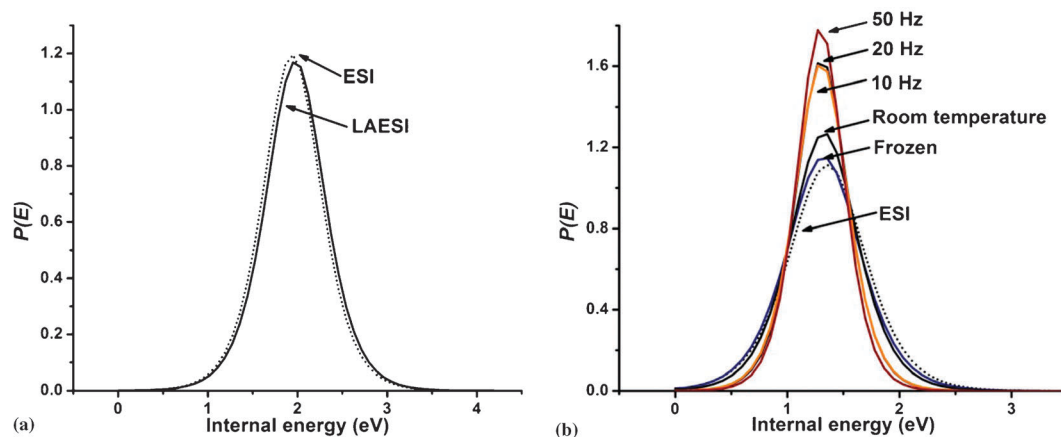


**Fig. 3** Internal energy deposition during mid-IR LAESI of leaf tissues using (a) an orthogonal acceleration TOF system at 60 V cone voltage, and (b) a Q-TOF system for ion detection. LAESI-generated ions had comparable internal energy distributions to ESI in both instrument configurations. Changes in laser repetition rate and sample temperature did not significantly alter the mean of the distributions, confirming low internal energy deposition for tissue samples in LAESI experiments. These uncorrected internal energy values do not reflect the ‘kinetic shift’ but indicate relative changes.

LAESI signal can be detected by moving the spray axis as far as 30 mm from the ablation spot.<sup>21</sup> Indeed, we can use our results to obtain a crude estimate of the size of the ejected droplets that contribute most to the LAESI signal. Inserting  $x_{\text{stop}} = 12$  mm into eqn (2) for the stopping distance, the distance where we have recorded the maximum LAESI signal in the present experiments yields  $2R = (9\mu x_{\text{stop}}/(2\rho v_0))^{1/2} \approx 5$   $\mu\text{m}$  for the effective diameter of the sample droplets. These droplets are sufficiently small to interact with the electrospray droplets that are known to have a diameter between 5  $\mu\text{m}$  and 10  $\mu\text{m}$  for similar spraying conditions.<sup>49</sup>

Our findings on energy deposition in LAESI can be compared to other atmospheric-pressure ionization techniques. For example, ESI, DESI, and sonic spray ionization (SSI) sources gave similar internal energy distributions with averages in the 1.7 to 1.9 eV range in ion trap systems,<sup>40</sup> and were slightly lower in paper spray<sup>39</sup> than in parallel ESI experiments. For solutions prepared with 50% methanol, Venturi-assisted array of micro-machined ultrasonic electrosprays gave similar results to ESI, whereas significantly lower  $\langle E \rangle$  was obtained when thermometer ions were analysed from water only.<sup>53</sup> Noticeably higher  $\langle E \rangle$  values were obtained under DART conditions with the average values 25 to 40% higher than the reference ESI case.<sup>41</sup>

These ion sources work with diverse sample types. Likewise, mid-IR ablation is oftentimes performed on targets that range from solutions to biological samples in LAESI experiments. It is therefore necessary to explore whether variations in the nature of the sample may manifest in changes in the extent of internal energy deposition into LAESI-generated ions.

#### Internal energy deposition in mid-IR ablation of tissues

Fast imaging experiments of mid-IR ablation revealed that variations in the physicochemical properties of samples translate into changes in the ablation mechanism. For example, secondary material ejection is not found for tissues with sufficiently high tensile strength.<sup>18</sup> Beyond differences in the physical properties, these structured samples may exhibit boundary conditions that can significantly differ from those of solutions. For example,

single cell ablation studies have recently revealed that cell walls in plant tissue confine the ablation process and delay the ejection of the cytosol.<sup>15</sup> Cell rupture was observed only after the second or third laser pulse, when the intracellular pressure exceeded the tensile strength of the cell wall. This process was different from the unobstructed ablation of solution samples. Furthermore, unlike in solution samples, the water content in tissues can vary significantly, an effect that modulates the energy coupling mechanism in mid-IR laser ablation. Whether these differences in sample properties alter the internal energy deposited into the molecular components of the ablation plume is unclear.

To address this question, ion internal energies were determined in LAESI experiments on tissues. Eight benzyl-substituted benzylpyridinium salts were air-dried onto the upper surface of *E. japonicus* leaves at  $\sim 100$   $\mu\text{g cm}^{-2}$  density and were directly ablated under experimental conditions that were similar to those discussed above. The obtained  $P(E)$  curves, presented in Fig. 3(a) together with direct ESI results, showed strong similarity between the internal energy distributions. At 60 V sampling cone potential, both the LAESI and ESI internal energy distributions exhibited a mean of  $\langle E \rangle = 2.10$  eV with similar widths.

The effects of the laser pulse repetition rate as well as the sample temperature were also investigated. The eight benzyl-substituted benzylpyridinium salts were individually deposited on leaf tissues and analyzed at 10 Hz, 20 Hz and 50 Hz repetition rates at ambient temperature. To explore the effect of target temperature, the experiment was repeated between 0 and  $-4$   $^{\circ}\text{C}$  using 10 Hz repetition rate. Based on the measured survival yields,  $P(E)$  distributions were obtained (see Fig. 3(b) and data from separate experiments in Table S2, ESI<sup>†</sup>). Changes in the repetition rate or cooling did not have detectable effects on the average internal energy,  $\langle E \rangle = 1.51$  eV. The widths of the distributions slightly decreased at increased repetition rates (see data in Table S2, ESI<sup>†</sup>). Thus, thermal activation of the sample was probably not a major factor in LAESI ionization.

## Internal energy and fragmentation of biomolecules

The LAESI and ESI experiments were extended to larger molecules known to fragment in laser desorption/ionization experiments. Unlike the thermometer ions, these molecules have multiple fragmentation channels and may require proton transfer for ionization. The samples included four peptides (des-tyrosine-leucine enkephalin, angiotensin II, bradykinin and substance P) as well as vitamin B<sub>12</sub>. In general, solutions of the peptides yielded singly, doubly, and triply charged protonated molecules without fragmentation. Comparisons of the representative mass spectra are shown in Fig. S2 (ESI†). Relative ion intensities in the acquired mass spectra demonstrated similarity between LAESI and ESI. The most significant difference was found for the intensity of the triply charged substance P molecule that showed significantly higher abundance in the LAESI experiment. Shifts in charge state distributions are known to occur in ESI based on, *e.g.*, differences in spraying modes. No indications of differences in ion internal energies were detected between LAESI and ESI of peptides.

Ion generation involving mid-IR ablation in LAESI was compared with UV laser desorption/ionization under MALDI conditions. Vitamin B<sub>12</sub> was reported to exhibit fragmentation pathways that were sensitive to the nature of the matrix and the laser fluence,<sup>54–57</sup> and was therefore a useful reference system. Mass spectra acquired for solution samples in LAESI and ESI experiments, as well as for dried samples by UV-MALDI using DHB as a matrix are compared in Fig. 4. No fragmentation was observed in the LAESI and the ESI experiments. This indicated that the particulates ejected during the second phase of the mid-IR laser ablation contained intact vitamin B<sub>12</sub> molecules. Both the LAESI and the ESI spectra exhibited predominantly doubly charged molecules. In contrast, the UV-MALDI spectra, acquired in vacuum, included several fragments, such as the ions  $m/z$  1329.6 and  $m/z$  972.2 that, on the basis of literature data, were assigned to  $[M-CN+H]^+$  and  $[M-CN-base-sugar-PO_4]^+$ ,

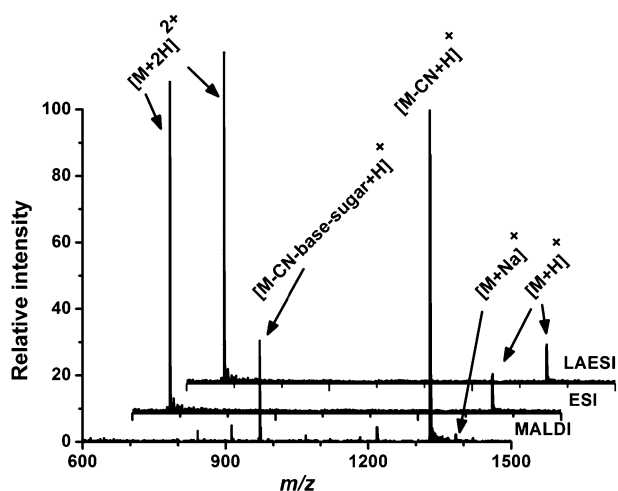


**Fig. 4** Mass spectra of vitamin B<sub>12</sub> produced by LAESI, ESI and UV-MALDI ionization. No fragmentation was observed in LAESI and ESI that produced singly ( $m/z$  1356.4) and predominantly doubly charged molecular ions ( $m/z$  678.2). In contrast, MALDI conditions gave rise to two major fragments (see labelled ions), indicating that UV excitation increased the internal energy of vitamin B<sub>12</sub>.

respectively.<sup>54,56</sup> The presence of these fragments, however, can be attributed to direct light absorption by the vitamin B<sub>12</sub> molecules at the laser wavelength, as the molar extinction coefficient of vitamin B<sub>12</sub> at the 361 nm absorption peak is  $27\,500\text{ M}^{-1}\text{ cm}^{-1}$ <sup>58</sup> that decays to still significant  $8371\text{ M}^{-1}\text{ cm}^{-1}$  at the 337 nm wavelength of the nitrogen laser.<sup>59</sup> Thus, these results alone do not demonstrate that compared to LAESI higher internal energies are produced in UV-MALDI desorption/ionization. It is interesting to note that fluence-dependent fragmentation has been reported in UV-MALDI,<sup>34,60</sup> laser desorption/ionization (LDI),<sup>61</sup> LISMA,<sup>36</sup> as well as NAPA ionization experiments.<sup>38</sup> Typical fluences in LAESI range has been between  $0.1$  to  $4\text{ J cm}^{-2}$ , thus the  $\sim 15\text{ J cm}^{-2}$  fluence used in these studies indicates that fragmentation is absent even at elevated fluences.

## 4. Conclusions

Despite the high temperature and pressure conditions associated with the sudden energy deposition and phase explosion present in mid-IR laser ablation of water-containing samples, solute molecules ejected in droplets or particulates were found to experience no appreciable gain in internal energy. Our survival yield experiments revealed that, compared to direct ESI, the recoil pressure induced material ejection in LAESI did not appreciably alter the internal energies of thermometer ions, peptides and vitamin B<sub>12</sub>. Sample phase (frozen vs. liquid), temperature and the repetition rate of the irradiation did not influence the internal energy distributions.

These fundamental findings have important implications for mid-IR laser ablation based sampling and analysis. As fragmentation of the solutes seems to be practically absent in LAESI experiments, the mass spectra reflect the molecular composition of the condensed phase samples. Even when LAESI is used for the direct sampling of very complex biological tissues and single cells, one can expect the absence of degradation during ablation. This, however, does not mean that the various chemical components are all represented in the spectra with equal propensity. Ion suppression effects due to competition for the available charges can still result in certain components being absent or underrepresented in the mass spectra.

In light of our findings, additional questions emerge. As all of our experiments are based on resonant coupling of the laser pulse energy into the target, it is unclear if ablation off of the resonance would yield similar results. For example, off resonance ablation can be efficiently performed by using ultrafast lasers with pulses in the femtosecond range<sup>57</sup> or by tuning the laser wavelength to wavelengths where linear absorption is negligible. Additional questions arise when the mean free path in the experiment becomes comparable to the dimensions of the ablation. This can be bought about by reducing the laser spot size (nanoscale ablation<sup>62</sup>) or by slightly reducing the pressure of the environment. As the shock wave dynamics dramatically changes under these conditions, the ejection of particulates and perhaps the internal energy of the produced ions are also expected to be affected. A deeper understanding of the mid-IR laser ablation mechanism of water-rich samples can propel the development of analytical and sample modification techniques of biological systems in their native or native-like environments.

## Acknowledgements

This material is based, in part, on work supported by the National Science Foundation under Grant Number 0719232 and by the Office of Basic Energy Sciences of the Department of Energy (DE-FG02-01ER15129). The authors are grateful for this financial support. The mention of commercial products, their sources, or their use in connection with material reported herein is not to be construed as either an actual or implied endorsement of such products by the Department of Health and Human Services.

## Notes and references

- 1 C. R. Phipps, *Laser ablation and its applications*, Springer, 2007.
- 2 M. R. Emmert-Buck, R. F. Bonner, P. D. Smith, R. F. Chuaqui, Z. P. Zhuang, S. R. Goldstein, R. A. Weiss and L. A. Liotta, *Science*, 1996, **274**, 998–1001.
- 3 R. K. Shori, A. A. Walston, O. M. Stafsuud, D. Fried and J. T. Walsh, *IEEE J. Sel. Top. Quantum Electron.*, 2001, **7**, 959–970.
- 4 R. G. Cooks, Z. Ouyang, Z. Takats and J. M. Wiseman, *Science*, 2006, **311**, 1566–1570.
- 5 J. Shiea, M. Z. Huang, H. J. HSu, C. Y. Lee, C. H. Yuan, I. Beech and J. Sunner, *Rapid Commun. Mass Spectrom.*, 2005, **19**, 3701–3704.
- 6 V. M. Doroshenko, V. V. Laiko, N. I. Taranenko, V. D. Berkout and H. S. Lee, *Int. J. Mass Spectrom.*, 2002, **221**, 39–58.
- 7 Y. Li, B. Shrestha and A. Vertes, *Anal. Chem.*, 2007, **79**, 523–532.
- 8 Y. Li, B. Shrestha and A. Vertes, *Anal. Chem.*, 2008, **80**, 407–420.
- 9 P. Nemes and A. Vertes, *Anal. Chem.*, 2007, **79**, 8098–8106.
- 10 Y. H. Rezenom, J. Dong and K. K. Murray, *Analyst*, 2008, **133**, 226–232.
- 11 J. S. Sampson, K. K. Murray and D. C. Muddiman, *J. Am. Soc. Mass Spectrom.*, 2009, **20**, 667–673.
- 12 P. Nemes, A. A. Barton and A. Vertes, *Anal. Chem.*, 2009, **81**, 6668–6675.
- 13 P. Nemes, A. S. Woods and A. Vertes, *Anal. Chem.*, 2010, **82**, 982–988.
- 14 B. Shrestha and A. Vertes, *Anal. Chem.*, 2009, **81**, 8265–8271.
- 15 B. Shrestha, P. Nemes and A. Vertes, *Appl. Phys. A: Mater. Sci. Process.*, 2010, **101**, 121–126.
- 16 B. Shrestha, J. M. Patt and A. Vertes, *Anal. Chem.*, 2011, **83**, 2947–2955.
- 17 A. Bogaerts, Z. Y. Chen, R. Gijbels and A. Vertes, *Spectrochim. Acta, Part B*, 2003, **58**, 1867–1893.
- 18 I. Apitz and A. Vogel, *Appl. Phys. A: Mater. Sci. Process.*, 2005, **81**, 329–338.
- 19 Z. Y. Chen, A. Bogaerts and A. Vertes, *Appl. Phys. Lett.*, 2006, **89**, 041503.
- 20 Z. Y. Chen and A. Vertes, *Phys. Rev. E: Stat., Nonlinear, Soft Matter Phys.*, 2008, **77**, 036316.
- 21 A. Vertes, P. Nemes, B. Shrestha, A. A. Barton, Z. Y. Chen and Y. Li, *Appl. Phys. A: Mater. Sci. Process.*, 2008, **93**, 885–891.
- 22 X. Fan and K. K. Murray, *Appl. Surf. Sci.*, 2009, **255**, 6297–6302.
- 23 R. W. Nelson, M. J. Rainbow, D. E. Lohr and P. Williams, *Science*, 1989, **246**, 1585–1587.
- 24 L. J. Romano and R. J. Levis, *J. Am. Chem. Soc.*, 1991, **113**, 9665–9667.
- 25 C. Collette, L. Drahos, E. De Pauw and K. Vekey, *Rapid Commun. Mass Spectrom.*, 1998, **12**, 1673–1678.
- 26 V. Gabelica and E. De Pauw, *Mass Spectrom. Rev.*, 2005, **24**, 566–587.
- 27 B. Shrestha, P. Nemes, J. Nazarian, Y. Hathout, E. P. Hoffman and A. Vertes, *Analyst*, 2010, **135**, 751–758.
- 28 H. I. Kentamaa and R. G. Cooks, *Int. J. Mass Spectrom. Ion Processes*, 1985, **64**, 79–83.
- 29 V. H. Wysocki, H. I. Kentamaa and R. G. Cooks, *Int. J. Mass Spectrom. Ion Processes*, 1987, **75**, 181–208.
- 30 F. Derwa, E. Depauw and P. Natalis, *Org. Mass Spectrom.*, 1991, **26**, 117–118.
- 31 S. Elizabeth, B. Kathrin and Z. Renato, *J. Mass Spectrom.*, 2000, **35**, 1035–1041.
- 32 G. H. Luo, I. Marginean and A. Vertes, *Anal. Chem.*, 2002, **74**, 6185–6190.
- 33 J. F. Greisch, V. Gabelica, F. Remacle and E. De Pauw, *Rapid Commun. Mass Spectrom.*, 2003, **17**, 1847–1854.
- 34 V. Gabelica, E. Schulz and M. Karas, *J. Mass Spectrom.*, 2004, **39**, 579–593.
- 35 G. H. Luo, I. Marginean, L. Ye and A. Vertes, *J. Phys. Chem. B*, 2008, **112**, 6952–6956.
- 36 J. A. Stolee, Y. Chen and A. Vertes, *J. Phys. Chem. C*, 2010, **114**, 5574–5581.
- 37 G. H. Luo, Y. Chen, H. Daniels, R. Dubrow and A. Vertes, *J. Phys. Chem. B*, 2006, **110**, 13381–13386.
- 38 J. A. Stolee and A. Vertes, *Phys. Chem. Chem. Phys.*, 2011, **13**, 9140–9146.
- 39 H. Wang, J. J. Liu, R. G. Cooks and Z. Ouyang, *Angew. Chem., Int. Ed.*, 2010, **49**, 877–880.
- 40 M. Nefliu, J. N. Smith, A. Venter and R. G. Cooks, *J. Am. Soc. Mass Spectrom.*, 2008, **19**, 420–427.
- 41 G. A. Harris, D. M. Hostetler, C. Y. Hampton and F. M. Fernandez, *J. Am. Soc. Mass Spectrom.*, 2010, **21**, 855–863.
- 42 J. W. Gauthier, T. R. Trautman and D. B. Jacobson, *Anal. Chim. Acta*, 1991, **246**, 211–225.
- 43 J. Laskin and J. H. Futrell, *Mass Spectrom. Rev.*, 2005, **24**, 135–167.
- 44 M. P. Sinha, A. Schultz and R. N. Zare, *J. Chem. Phys.*, 1973, **58**, 549–556.
- 45 L. Drahos, R. M. A. Heeren, C. Collette, E. De Pauw and K. Vekey, *J. Mass Spectrom.*, 1999, **34**, 1373–1379.
- 46 Z. Takats, L. Drahos, G. Schlosser and K. Vekey, *Anal. Chem.*, 2002, **74**, 6427–6429.
- 47 V. Gabelica, E. De Pauw and M. Karas, *Int. J. Mass Spectrom.*, 2004, **231**, 189–195.
- 48 A. Pak, D. Lesage, Y. Gimbert, K. Vekey and J. C. Tabet, *J. Mass Spectrom.*, 2008, **43**, 447–455.
- 49 P. Nemes, I. Marginean and A. Vertes, *Anal. Chem.*, 2007, **79**, 3105–3116.
- 50 P. Lecchi, J. H. Zhao, W. S. Wiggins, T. H. Chen, P. F. Yip, B. C. Mansfield and J. M. Peltier, *J. Am. Soc. Mass Spectrom.*, 2009, **20**, 398–410.
- 51 R. D. Voyksner and T. Pack, *Rapid Commun. Mass Spectrom.*, 1991, **5**, 263–268.
- 52 D. J. Rousell, S. M. Dutta, M. W. Little and K. K. Murray, *J. Mass Spectrom.*, 2004, **39**, 1182–1189.
- 53 C. Y. Hampton, C. J. Silvestri, T. P. Forbes, M. J. Varady, J. M. Meacham, A. G. Fedorov, F. L. Degertekin and F. M. Fernandez, *J. Am. Soc. Mass Spectrom.*, 2008, **19**, 1320–1329.
- 54 L. He, G. Wei and K. K. Murray, *J. Am. Soc. Mass Spectrom.*, 1997, **8**, 140–147.
- 55 G. R. Kinsel, L. M. Preston and D. H. Russell, *Biol. Mass Spectrom.*, 1994, **23**, 205–211.
- 56 J. F. Blankenship, M. J. VanStipdonk and E. A. Schweikert, *Rapid Commun. Mass Spectrom.*, 1997, **11**, 143–147.
- 57 J. J. Brady, E. J. Judge and R. J. Levis, *Rapid Commun. Mass Spectrom.*, 2009, **23**, 3151–3157.
- 58 J. A. Hill, J. M. Pratt and R. J. P. Williams, *J. Chem. Soc., London*, 1964, **1964**, 5149–5153.
- 59 H. Du, R. C. A. Fuh, J. Z. Li, L. A. Corkan and J. S. Lindsey, *Photochem. Photobiol.*, 1998, **68**, 141–142.
- 60 A. Vertes, G. H. Luo, L. Ye, Y. Chen and I. Marginean, *Appl. Phys. A: Mater. Sci. Process.*, 2004, **79**, 823–825.
- 61 S. Dagan, Y. Hua, D. J. Boday, A. Somogyi, R. J. Wysocki and V. H. Wysocki, *Int. J. Mass Spectrom.*, 2009, **283**, 200–205.
- 62 R. Stockle, P. Setz, V. Deckert, T. Lippert, A. Wokaun and R. Zenobi, *Anal. Chem.*, 2001, **73**, 1399–1402.

Electronic Supplementary Information for

## Internal energy deposition and ion fragmentation in atmospheric-pressure mid-infrared laser ablation electrospray ionization

Peter Nemes,<sup>1</sup> Hehua Huang, and Akos Vertes\*

Department of Chemistry, The George Washington University, Washington, DC 20052

\*Corresponding author address: Department of Chemistry, The George Washington University, Washington, DC 20052, USA. E-mail: [vertes@gwu.edu](mailto:vertes@gwu.edu); Fax: +1 202-994-5873; Tel: +1 202-994-2717

Initially, the ion transfer region of the mass spectrometer was characterized in survival yield (SY) experiments. The collected SY data were plotted as a function of the critical bond energies (see Table S1) to produce the sigmoidal curves in Figure S1a and to determine the internal energy distributions,  $P(E)$ , of the generated ions (see Figure S1b). Increasing potential differences between the sampling and skimmer cones of the TOF instrument lead to decreasing the SY values, i.e., to shifting of the sigmoidal curves to higher critical energies (see Figure S1a). The calculated  $P(E)$  reveals that higher sampling cone potentials increased the average internal energies of the thermometer ions for both ESI and LAESI conditions (see Figure 1b). The means and the widths of the computed distributions, tabulated in Table S2, confirmed that LAESI and ESI generated ions with similar internal energies.

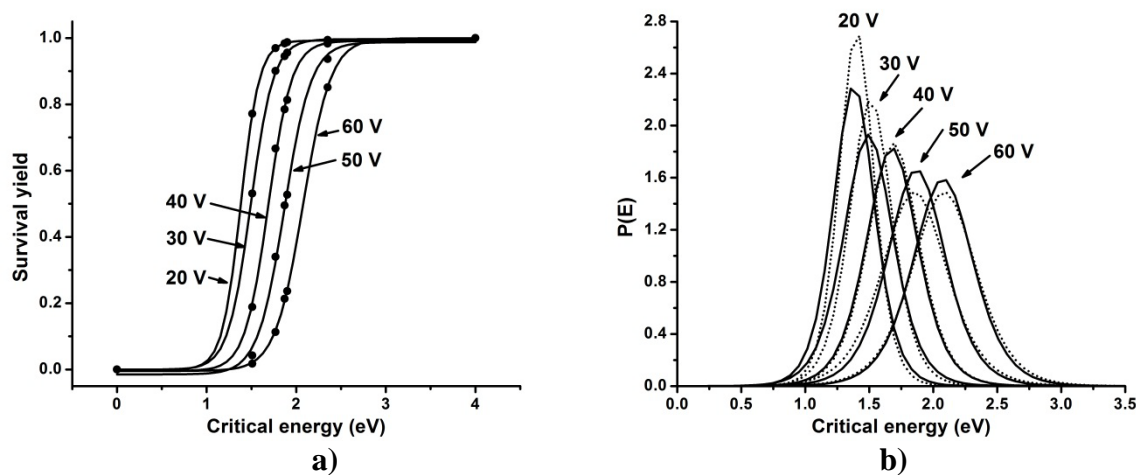


**Figure S1.** a) Sigmoidal SY curves for LAESI and b) internal energy distributions for ESI (dotted curves) and LAESI (solid curves) at different cone voltages. The extent of internal energy deposition by LAESI was indistinguishable from ESI, revealing a similarity in energy

<sup>1</sup>Current address: US Food and Drug Administration, 10903 New Hampshire Ave. #64-3068, Silver Spring, MD 20993, USA. E-mail: [Peter.Nemes@fda.hhs.gov](mailto:Peter.Nemes@fda.hhs.gov); Tel: +1 301-796-3366

deposition in ion generation. Fitting parameters are summarized in Table S2. Error bars are within symbols.

Ion generation was also evaluated for large biomolecules with multiple potential fragmentation channels. Figure S2 shows the mass spectra obtained for the peptides substance P and angiotensin II. Both LAESI and ESI generated singly, doubly, and triply charged ions. No fragmentation was detected with either method. Ions in the low  $m/z$  region ( $m/z < 300$ ) in Figures S2a and S2d correspond to the background from the electrospray solvent.

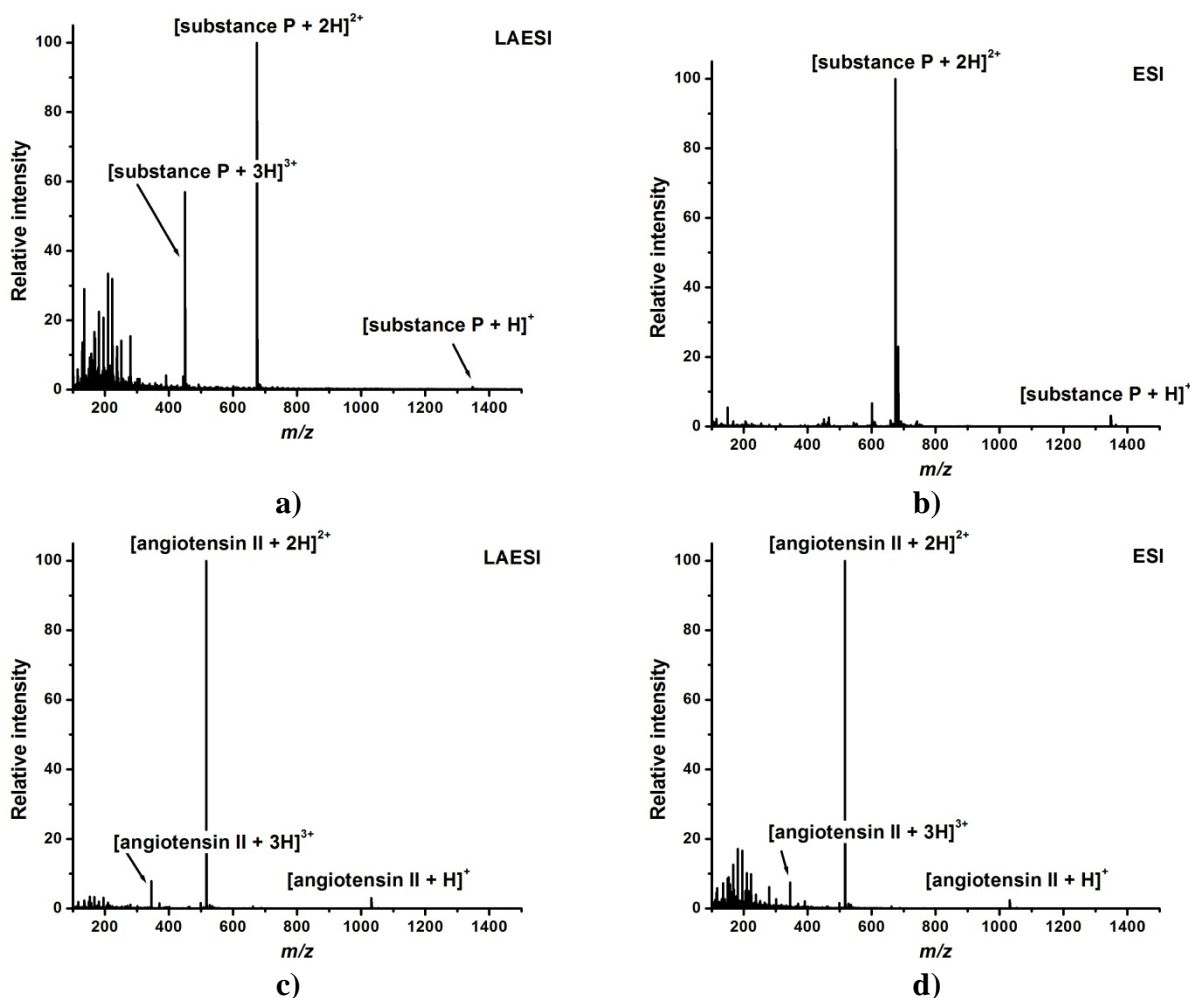


**Figure S2.** Comparison of peptide mass spectra in LAESI and ESI experiments. Both **a)** LAESI and **b)** ESI of substance P yielded singly ( $m/z$  1347.7), doubly ( $m/z$  674.4), and triply ( $m/z$  449.9) charged species. Similarly, **c)** LAESI and **d)** ESI of angiotensin II solutions gave singly ( $m/z$  1031.5), doubly ( $m/z$  516.3), and triply charged ( $m/z$  344.5) ions. No significant fragmentation was observed with either ionization method.

**Table S1.** Benzyl-substituted benzylpyridinium ions and their critical bond energies,  $E_b$ , calculated using AM1 in References <sup>1,2</sup>.

Substituent of thermometer ion	Abbreviation	$E_b$ (eV)	$m/z$ ( $M^+$ )	$m/z$ ( $F^+$ )
4-nitro-	4NO <sub>2</sub>	2.35	215.1	136.0
3-methoxy-	3MO	1.95	200.1	121.1
4-chloro-	4Cl	1.90	204.1	125.0
3-methyl-	3M	1.90	184.1	105.1
4-fluoro-	4F	1.87	188.1	109.1
2-methyl-	2M	1.80	184.1	105.1
4-methyl-	4M	1.77	184.1	105.1
4-methoxy-	4MO	1.51	200.1	121.1

**Table S2.** Nonlinear regression results on measured survival yield data and calculated internal energy distribution parameters.

Instrument	Sampling cone potential* (V)	Sample phase	$T_{\text{sample}}$ (°C)	Laser repetition rate (Hz)	Regression coefficient for sigmoidal fit		Mean and (width) of Gaussian (eV)	
					ESI	LAESI	ESI	LAESI
TOF MS	20	solution	25	10	0.997	0.999	1.40 (0.28)	1.38 (0.37)
	30	solution	25	10	0.997	0.999	1.51 (0.35)	1.49 (0.40)
	40	solution	25	10	0.997	0.998	1.68 (0.42)	1.69 (0.41)
	50	solution	25	10	0.983	0.997	1.85 (0.52)	1.87 (0.46)
	60	solution	25	10	0.998	0.999	2.09 (0.52)	2.08 (0.49)
	60	tissue	25	10	0.944	0.953	1.94 (0.64)	1.98 (0.65)
Q-TOF MS	8	tissue	0	10	-	0.994	-	1.53 (0.61)
	8	tissue	25	10	-	0.998	-	1.51 (0.41)
	8	tissue	25	20	-	0.998	-	1.51 (0.40)
	8	tissue	25	50	-	0.996	-	1.51 (0.42)
	8	solution	25	10	0.99129	-	1.57 (0.64)	-

\*The sampling cone potential measures the sampling cone potential against the skimmer cone in the TOF MS instrument, whereas it denotes the potential applied against earth ground in the Q-TOF MS system.

## References

- [1] Gabelica, V.; De Pauw, E. Karas, M., *Int. J. Mass Spectrom.* **2004**, *231*, 189-195.  
 [2] Gabelica, V. De Pauw, E., *Mass Spectrometry Reviews* **2005**, *24*, 566-587.